Triple Helix Forming TRIPside Molecules That Target Mixed Purine/Pyrimidine DNA Sequences†

Jian-Sen Li,‡ Ronald Shikiya,§ Luis A. Marky,‡,§ and Barry Gold*,‡,§

Eppley Institute for Research in Cancer and Department of Pharmaceutical Sciences, University of Nebraska Medical Center, Omaha, Nebraska 68198-680

Received September 12, 2003; Revised Manuscript Received December 5, 2003

ABSTRACT: A new strategy to form stable and sequence-specific triple helical DNA structures at mixed purine/pyrimidine sequences using a combination of four C-glycosides (TRIPsides) has been described [Li et al. (2003) *J. Am. Chem. Soc. 125*, 2084]. The partial realization of the approach is demonstrated by incorporating two of the four TRIPsides into oligomers that can potentially fold into intramolecular triplexes that contain one or two major groove crossovers of the purine Hoogsteen H-bond information. Using temperature-dependent electronic and fluorescence spectroscopy and differential scanning calorimetry, it is demonstrated that stable triplexes form at physiological conditions at non-homopurine targets. In addition, triplexes using the TRIPsides form in a highly sequence specific manner.

The inability to form stable structures in a sequence-specific manner at mixed purine/pyrimidine sequences is the major deterrent in the development of antigene approaches based on triple helix DNA formation. This problem arises because the triplex forming oligomer (TFO) binds asymmetrically in the major groove with its backbone close to that of the purine strand with which it associates via Hoogsteen H-bonding (*1*−*6*). At mixed purine/pyrimidine sequences, the TFO cannot read with continuity Hoogsteen H-bonding information on the purine nucleobases because this requires the TFO to traverse back and forth across the major groove. This is not structurally possible. Reading purine H-bonding information on both strands also requires that the TFO be insensitive to strand polarity; however, both the pyrimidine (*7*−*10*) and purine (*11*−*14*) motifs for DNA triplexes have strong unidirectional polarity requirements. Recently, we proposed a set of four C-glycosides, i.e., TRIPsides (*15*), based on 2-aminoquinoline and 2-aminoquinazoline heterocycles (Figure 1), that are designed to differentiate between the four base pairing schemes in the major groove, i.e., G:C, C:G, A:T, and T:A, and to "read" Hoogsteen base pairing information on both strands without having to change strand polarity (*16*). The feasibility of the approach was initially demonstrated for a TFO that folds into an intramolecular triplex with both sequence and orientational specificity with a $d(T)_6$:$d(A)_6$ duplex. A critical test of the TRIPside design is the ability to form triplexes at mixed purine/pyrimidine sequences. The results of UV−visible melting, differential scanning calorimetry (DSC), and fluorescence studies presented herein provide evidence that

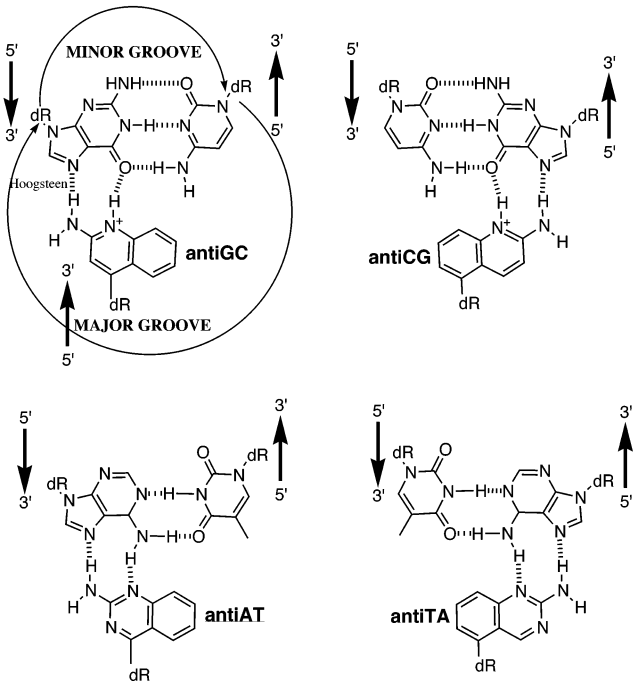

FIGURE 1: Structures of the 2-aminoquinazoline (antiTA and antiAT) and 2-aminoquinoline (antiGC and antiCG) TRIPsides associated with their Watson−Crick duplex targets: only antiGC and antiTA were used in the current studies.

TFO's composed of two of the TRIPsides can be targeted to mixed DNA sequences to yield stable and sequence specific triplex structures under physiological conditions.

EXPERIMENTAL PROCEDURES

All reagents were of the highest grade commercially available and used without any purification. The synthetic scheme is shown in Figure 2.

Synthesis of 2-Amino-4-hydroxyquinoline. Anilinium toluene-*p*-sulfonate (53 g) is heated at 260 °C for 5 min under N_2

† This work was supported by NIH Grant RO1 CA29088 and Cancer Center Support Grant P30 CA36727 from the National Cancer Institute.

* To whom correspondence should be addressed. Eppley Institute for Research in Cancer, University of Nebraska Medical Center, 986805 Nebraska Medical Center, Omaha, NE 68198-6805; voice, 402-559-5148; fax, 402-559-4651; e-mail, bgold@unmc.edu.

‡ Eppley Institute for Research in Cancer.

§ Department of Pharmaceutical Sciences.

10.1021/bi035648d CCC: $27.50
Published on Web 01/24/2004

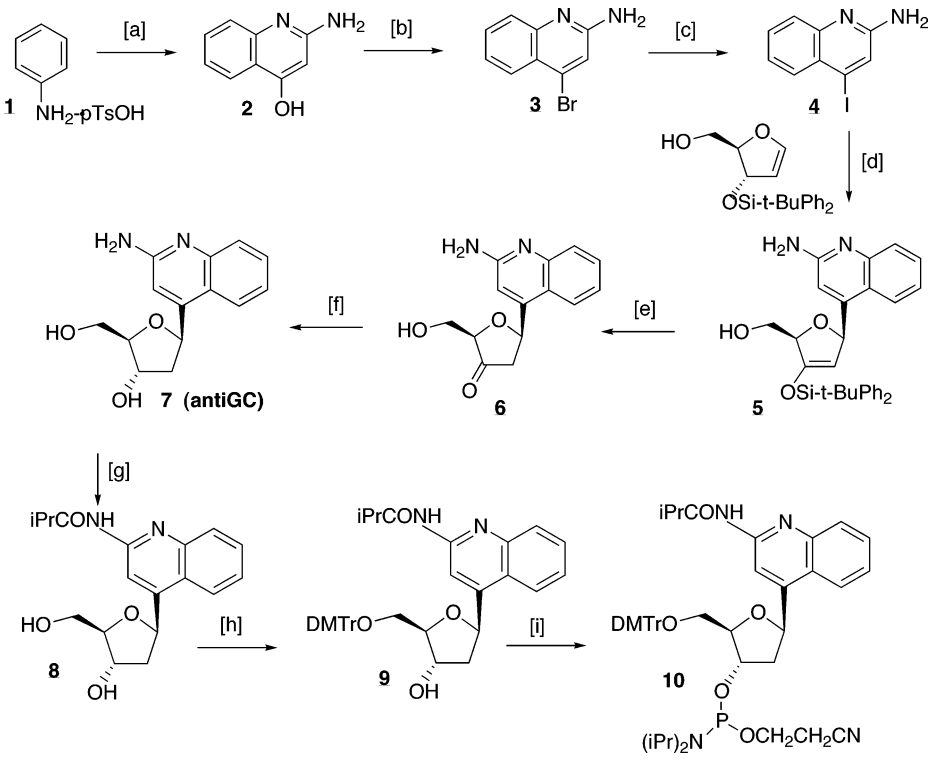

FIGURE 2: Synthesis of antiGC phosphoramidite: [a] NC-CH_2CO_2Et; [b] $POBr_3/PBr_3$, 140−160 °C; [c] $KI/I_2/Ni$, 95 °C; [d], bis(dibenzylideneacetone)Pd(0), $(t\text{-}Bu)_3P/Et_3N$, THF, reflux; [e] TBAF, 0 °C; [f] $NaHB(OAc)_3$, HOAc/MeCN, −23 °C; [g] $(i\text{-}PrCO)_2O$, pyridine; [h] DMTr-Cl, pyridine, 0 °C; [i] 2-cyanoethyl *N*,*N*-diisopropylchlorophosphoramidite, *N*,*N*-diisopropylethyl-amine, CH_2Cl_2, 0 °C.

and ethyl cyanoacetate (22.6 g) is added dropwise through an air-condenser within 5 min. Then the temperature of the reaction is allowed to drop to 220−250 °C, and after 75 min the orange slurry is cooled, 75−100 mL of $CHCl_3$ is added, and the resulting mixture is refluxed overnight to dissolve the solid. This solution is vigorously mixed with H_2O (60 mL), EtOH (30 mL), and saturated Na_2CO_3 solution (50 mL). The resulting slurry is filtered, and the product, a pale-yellow solid, is dried in vacuo over P_2O_5 (10.5 g, 30% yield). The remaining filtrate can be partially concentrated to obtain additional product: mp 260 °C (lit. mp 258−259 °C (decomp.) (*17*); ^1H NMR (DMSO-d_6): δ 5.22 (s, 1 H), 6.12 (bs, 2 H, NH_2), 7.10 (dd, 1 H, J = 7.5 and 1.5), 7.25 (d, 1 H, J = 7.5), 7.43 (dd, 1 H, J = 7.5 and 1.5), 7.88 (d, 1 H, J = 7.5), 10.62 (s, 1 H, OH); HRMS (FAB) *m*/*z* 160.0636 (M^+), 160.0637 (calcd).

Synthesis of 2-Amino-4-bromoquinoline (***3***). **2** (11.13 g) is heated with $POBr_3$ (22.0 g, 1.1 equiv) in PBr_3 (1.5 equiv) at 140−160 °C under N_2 for 19 h. The reaction is cooled, basified with 2 M NaOH (250 mL), and thrice extracted with $CHCl_3$ (30 mL). The organic layer is concentrated, and the residue is purified by silica gel chromatography using $CHCl_3$/acetone/Et_3N (25:25:1) to afford the crude product that is crystallized from benzene/hexane to furnish dark red prism crystals (13.0 g, 84%): mp 137−138 °C; ^1H NMR ($CDCl_3$) δ 4.86 (bs, 2 H, NH_2), 7.05 (s, 1 H), 7.33 (dd, 1 H, J = 6.5, 1.5), 7.58 (dd, 1 H, J = 6.5, 1.5), 7.62 (d, 1 H, J = 6.5), 7.96 (d, 1 H, J = 6.5); HRMS (FAB) *m*/*z* 221.9803 (M^+), 221.9793 (calcd).

Synthesis of 2-Amino-4-iodoquinoline (***4***). **3** (7.67 g) is heated with KI (29 g, 3 equiv.), Ni metal powder (10 g, 5.5 equiv), and I_2 (240 mg, 1% of Ni metal powder) in DMF (70 mL) at 95 °C for 48 h, then at 180 °C for 15 min. The DMF is removed in vacuo and the residue subjected to silica gel chromatography with EtOAc/Et_3N (100:1) to give the desired product (9.1 g, 98%). An analytical sample was recrystallized from benzene/hexane to furnish dark red needles: mp 131−132 °C; ^1H NMR ($CDCl_3$): δ 4.91 (bs, 2 H, NH_2), 7.06 (s, 1 H), 7.33 (dd, 1 H, J = 6.5, 1.5), 7.58 (dd, 1 H, J = 6.5, 1.5), 7.62 (d, 1 H, J = 6.5), 7.97 (d, 1 H, J = 6.5); HRMS (FAB) *m*/*z* 269.9658 (M^+), 269.9654 (calcd).

*Synthesis of 4-[β-*D*-Glyceropentofuran-3′-ulos-1′-yl]-2-aminoquinoline* (***6***). 1,4-Anhydro-3-*O*-(*tert*-butyldiphenylsilyl)-2-deoxy-D-erythro-pent-1-enitol (*18*) (2.79 g) and **4** (1.86 g) are dissolved in dioxane (110 mL) under N_2. Then a catalytic amount of bis(dibenzlideneacetone)Pd(0) (0.81 g) and $(t\text{-}Bu)_3P$ (0.71 mL) are added to the reaction. After the reaction is purged with N_2 for 15 min, Et_3N (7 mL) is added. The final mixture is then refluxed under N_2 for 12 h, and the reaction is cooled, filtered, and the filtrate is concentrated in vacuo. The residue is purified by silica gel chromatography with CH_2Cl_2/MeOH/Et_3N (gradient from 100:2:1 to 100:5:1) to give the desired nucleoside and the quinoline−quinoline dimer side-product in a ratio 3:2 (total 2.14 g). This mixture is dissolved in THF (10 mL) containing HOAc (0.6 mL) and Bu_4NF (4 mL, 1 M in THF) and stirred at 0 °C for 50 min. Then NH_4OH (2 mL) is added, and the solution is concentrated in vacuo. The residue is subjected to silica gel column chromatography with CH_2Cl_2/MeOH/Et_3N (gradient from 100:3:1 to 100:17:1) to give the desired desilylated product (0.45 g, 25% overall yield): ^1H NMR ($CDCl_3$): δ 2.37 (dd, 1 H, J = 12.0, 11.0, C2′-H), 3.07 (dd, 1 H, J = 12.0, 11.0, C2″-H), 3.73−4.11 (m, 2 H, C5′-H, C5″-H), 4.16 (bs, 1 H, C4′-H), 5.62 (m, 1 H, C1′-H), 7.20 (m, 1 H), 7.35 (m, 1 H), 7.50 (s, 1 H), 7.52 (m, 1 H), 7.73 (m, 1 H); HRMS (FAB) *m*/*z* 259.1072 (MH^+), 259.1083 (calcd).

*Synthesis of 4-[2′-Deoxy-β-D-threo-pentofuranosyl]-2-aminoquinoline (antiGC) (**7**).* **6** (1.33 g) is dissolved in 120 mL of AcOH:CH_3CN (1:1) and stirred under N_2 at −23 °C in a solid CO_2 + CCl_4 bath. $NaHB(OAc)_3$ (1.5 g) is added to the cooled solution and the mixture stirred at −23 °C for 75 min. The reaction is concentrated and stirred with Na_2CO_3 (5.14 g) in CH_2Cl_2/MeOH (1:1, 50 mL) at room-temperature overnight, and the material is chromatographed on silica gel using CH_2Cl_2/MeOH/Et_3N (gradient from 100:2:1 to 100:50:1). The crude product is obtained as a pale yellow powder and is further purified by crystallization from a mixture of benzene/CH_2Cl_2/*i*PrOH/Et_3N (20:30:2:1) to yield a white powder (1.29 g, 96% yield): mp > 150 °C (decomp.); ^{1}H NMR (DMSO-d_6): δ 1.72−1.77 (m, 1 H, C2′-H), 2.35−2.39 (m, 1 H, C2″-H), 3.43−3.59 (m, 2 H, C5′-H, C5″-H), 3.88 (bs, 1 H, C4′-H), 4.20 (bs, 1 H, C3′-H), 5.54 (dd, 1 H, J = 4.0, 6.0, C1′-H), 6.38 (s, 2 H, NH_2), 6.95 (s, 1 H), 7.15 (t, 1 H, J = 5.5), 7.42−7.46 (m, 2 H), 7.67 (d, 1 H, J = 6.0); HRMS (FAB) m/z 261.1231(MH^+), 261.1240 (calcd).

*Synthesis of N^2-Isobutyryl-4-[2′-deoxy-β-D-threo-pentofuranosyl]-2-aminoquinoline (**8**).* **7** (0.40 g) in dry pyridine (20 mL) is cooled in an ice bath and treated with TMS-Cl (1 mL) under N_2. The reaction is stirred at 0 °C for 30 min, then *iso*butyric anhydride (1.35 mL) is added, and the reaction is stirred for an additional 2 h at room temperature under N_2. The reaction is then cooled in an ice bath and cold H_2O (2.5 mL) added. After 15 min, concentrated NH_4-OH (2.5 mL) is added to give a solution approximately 2 M in NH_3. This mixture is stirred for another 30 min in an ice bath and then concentrated under reduced pressure to afford an oil that is purified on silica gel with CH_2Cl_2/MeOH/Et_3N (100:10:1) to furnish the desired product as a pale yellow solid (0.4 g, 79% yield): ^{1}H NMR ($CDCl_3$) δ 1.15 (d, J = 6.5, 6 H), 2.12−2.18 (m, 1 H, C2′-H), 2.60−2.65 (m, 2 H, including C2″-H), 3.83 (dd, 1 H, J = 8.0, 4.5, C5′-H), 4.01 (dd, 1 H, J = 8.0, 4.5, C5″-H), 4.21 (dd, 1 H, J = 8.0, 3.5, C4′-H), 4.55 (q, 1 H, J = 5.5, 3.5, C3′-H), 5.92 (dd, 1 H, J = 2.5, 7.0, C1′-H), 7.29 (s, 1 H), 7.47 (dd, 1 H, J = 1.5, 8.5), 7.68 (dd, 1 H, J = 1.5, 8.5), 7.86 (d, 1 H, J = 8.5), 7.88 (d, 1 H, J = 8.5), 8.69 (s, 1 H); HRMS (FAB) m/z 353.1474 ([M + Na]$^+$), 353.1580 (calcd).

*Synthesis of N^2-Isobutyryl-4-[2′-deoxy-β-D-threo-pentofuranosyl-5′-O-(4,4′-dimethoxytrityl)]-2-aminoquinoline (**9**).* Isobutyrate **8** (0.17 g) is dissolved in dry pyridine (5 mL) under a N_2 atmosphere. Then 4,4′-dimethoxytrityl chloride (0.23 g) and Et_3N (0.2 mL) are added to the solution at room temperature. Another aliquot of trityl chloride and Et_3N is added after 3 h, and the reaction is stirred under N_2 at room temperature for a total of 20 h. After concentration of the sample, the residue is dissolved in $CHCl_3$ (30 mL) and washed thrice with saturated $NaHCO_3$ (30 mL) and thrice with H_2O (30 mL). The solution is concentrated, and the residue is chromatographed on silica gel with CH_2Cl_2/MeOH/Et_3N (100:2:1). The final product, which was crystallized from Et_2O/hexane, is a white solid (0.24 g, 74% yield): ^{1}H NMR ($CDCl_3$) δ 1.26 (d, J = 7.0, 6 H), 2.20−2.25 (m, 1 H, C2′-H), 2.48−2.53 (m, 1 H, C2″-H), 2.56−2.62 (m, 1 H), 3.38 (dd, 1 H, J = 10.0, 4.5, C5′-H), 3.53 (dd, 1 H, J = 10.0, 4.5, C5″-H), 3.77 (s, 6 H), 4.08−4.10 (m, C4′-H), 4.44 (bs,1 H, C3′-H), 5.75 (dd, 1 H, J = 4.0, 7.5, C1′-H), 6.80−6.86 (m, 3 H), 7.24−7.43 (m, 12 H), 7.62 (dd, 1 H, J = 1.5, 8.5), 7.81 (d, 1 H, J = 8.5), 8.04 (d, 1 H, J = 8.5), 8.57 (s, 1 H); HRMS (FAB) m/z 655.2806 ([M + Na]$^+$), 655.2784 (calcd).

*Synthesis of N^2-Isobutyryl-4-[2′-deoxy-β-D-threo-pentofuranosyl-3′-O-(2-cyanoethoxy)(diisopropylamino)phosphino-5′-O-(4,4′-dimethoxytrityl)]-2-aminoquinoline (**10**).* The trityl compound **9** (0.26 g) is dissolved in CH_2Cl_2 (10 mL) and cooled in an ice bath under N_2 atmosphere. Then Hunig base (0.4 mL) is added followed by 2-cyanoethyl-*N*,*N*-diisopropylphosphoramidite (0.15 mL). The reaction is stirred at 0 °C for 10 min, and then at room temperature for 75 min. After concentration in vacuo, the residue is dissolved in $CHCl_3$ (30 mL), and washed thrice with saturated $NaHCO_3$ solution (30 mL) and thrice with H_2O (30 mL). The organic phase is concentrated, and the residue is chromatographed on silica gel with CH_2Cl_2/hexane/Et_2O/Et_3N (50:100:150:3). The final product is a pale yellow powder (0.3 g, 88% yield): ^{1}H NMR ($CDCl_3$) δ 1.05−1.28 (m, 14 H), 1.46 (d, 6 H, J = 7.0), 2.20−2.24 (m, 1 H, C2′-H), 2.46−2.68 (m, 3 H, C2″-H), 3.38−3.42 (m, 2 H, C5′-H, C5″-H), 3.58−3.62 (m, 1 H), 3.76 (s, 6 H), 4.24 (bs, 1 H, C4′-H), 4.58 (bs,1 H, C3′-H), 5.76 (m, 1 H, C1′-H), 6.80−6.86 (m, 3 H), 7.24−7.43 (m, 12 H), 7.62 (dd, 1 H, J = 1.5, 8.5), 7.83 (d, 1 H, J = 8.5), 8.13 (d, 1 H, J = 8.5), 8.61 (s, 1 H); HRMS (FAB) m/z 833.4049 (MH^+), 833.4044 (calcd).

*pK_a of antiGC (**7**).* To TRIPside **7** (51.5 μM) dissolved in H_2O is added NaOAc buffer to give solutions with measured pH values of 3.93, 5.34, 5.90, 6.32, 6.68, 6.93, 7.29, 7.36, 7.44, and 9.58. The UV spectra of these solutions were recorded from 200 to 400 nm. The UV spectra at the different pH values were analyzed by plotting A_{237} as a function of pH to calculate the pK_a.

Preparation of Oligomers. The 200 nmol scale synthesis of the oligomers were performed using standard solid-phase phosphoramidite chemistry on an ABI 394 instrument. A 0.1 M CH_3CN solution of phosphoramidite (**10**) is used with coupling times of 7 min, which gives >99% coupling efficiency. After the synthesis, the resin inside the cartridge is mixed with 1 mL of concentrated NH_4OH, placed in a sealed bottle, and deprotected at 55 °C for 8 h. The crude oligomers were purified by HPLC: flow rate, 4 mL/min; solvent, 0.1 M Et_3N/HOAc (TEAA) (pH 7.0)/CH_3CN (9:1) for 10 min, to 0.1 M TEAA (pH 7.0)/CH_3CN (3:2) over 15 min, and then to 100% CH_3CN over 5 min. The HPLC fractions containing the oligomer were combined and lyophilized, and the residue was detritylated with 80% HOAc (30 μL per OD) at room temperature for 20 min. The final product was purified on a Sephadex G-10 column and confirmed by MALDI-TOF MS.

NMR Conformational Studies. The conformational analysis of the antiTA and antiGC TRIPsides was determined by ^{1}H NMR on a Varian INOVA 500-MHz Spectrometer using NOESY with presaturation field strength γB_1 of 50 Hz and a mixing time of 0.4 s at 25 °C in 10 mM sodium phosphate buffer (pH 7.0) in D_2O containing 50 mM NaCl. For antiTA TRIPside, the sample concentration was 19.2 mM, and the relaxation delay for the NOESY experiment was 2.0 s. For antiGC, the sample concentration was 14.4 mM, and the relaxation delay was 2.7 s.

Thermal Denaturation Studies. Melting curve transition measurements were performed on an AVIV 14 DS UV/Vis spectrometer equipped with an IBM computer as thermoprogrammer. Oligomers (3−6 μM strand concentration) are

dissolved in 10 mM sodium phosphate buffer (pH 7.0, unless stated otherwise) containing 50 mM NaCl. The oligomers are heated to 80 °C and slowly cooled to 0 °C, and held at that temperature for 30 min. The temperature is scanned from 0 to 80 °C with data-point collection in intervals of 0.2 °C. Below 20 °C, the cell compartment is flushed with N_2 to avoid condensation of H_2O on the UV cells. The unfolding of the oligomers was measured by the change in absorbance at 260, 330, and 350 nm versus temperature. The transition temperature T_M was determined as the first derivative of the melting curve and confirmed by shape analysis (*19*).

Fluorescent Studies. Fluorescence emission spectra were recorded at 0 and 88 °C from 330 to 600 nm with data-point collection in intervals of 2 nm on an AVIV Automated Titrating Differential/Ratio spectrofluorometer (model ATF105) with a fixed excitation wavelength at 350 nm. The emission and excitation slits were set at 5 nm. The concentration of oligomers was 3−6 μM in 10 mM sodium phosphate buffer (pH 7.0) containing 50 mM NaCl. The oligomer solutions are heated to 88 °C and the spectrum is recorded, and then slowly cooled to 0 °C, held at 0 °C for 1 h, and the spectrum is re-recorded.

Differential Scanning Calorimetry (DSC). Heat capacity functions of the triplex or duplex to coil transition of the oligomers were measured using a Microcal VP-DSC differential scanning calorimeter (Northampton, MA). Two cells, the sample cell containing 0.6 mL of an oligomer solution (80 μM) and the reference cell filled with the same volume of buffer solution, were heated from 0 to 110 °C at a heating rate of 0.75 °C/min. Analysis of the resulting thermograms yielded transition temperatures, T_M's, and standard thermodynamic profiles for the unfolding of each molecule (*19*). A typical experiment consists of obtaining a heat capacity profile of a DNA solution against a buffer solution. This experimental curve is normalized by the heating rate after first subtracting a buffer versus buffer scan. Integration of the resulting curve, $\int \Delta Cp\mathrm{d}T$, and normalization for the number of moles yields the molar unfolding enthalpy, ΔH_{cal}, which is independent of the nature of the transition. The molar entropy, ΔS_{cal} is obtained by a similar procedure, $\int(\Delta Cp/T)\mathrm{d}T$. The free energy at any temperature T is then obtained with the Gibbs equation: $\Delta G^\circ_{cal}(T) = \Delta H_{cal} - T\Delta S_{cal}$, which assumes similar heat capacities for the hairpin and random coil states. Alternatively, $\Delta G^\circ_{cal}(T)$ is obtained using the following relationship: $\Delta G^\circ_{cal}(T) = \Delta H_{cal}(1 - T/T_M)$, which is rigorously true for intramolecular transitions. Both methods yielded similar values.

RESULTS

Conformational Analysis. Implicit in the recognition of specific Watson−Crick duplex sequences by the aminoquinoline and aminoquinazoline bases is the requirement that the heterocyclic rings adopt an *anti*-conformation with respect to the deoxyribose ring (*16*). If there is appreciable population of the *syn*-isomer, antiGC and antiTA would be pseudo-equivalent to antiCG and antiAT, respectively (Figure 3). To experimentally determine the conformational preference of the heterocyclic rings, ^{1}H NMR NOESY experiments were performed in aqueous buffer (pH 7.0) at room temperature. The spectrum of the antiTA TRIPside shows a strong NOE between the H-4 proton on the aromatic ring

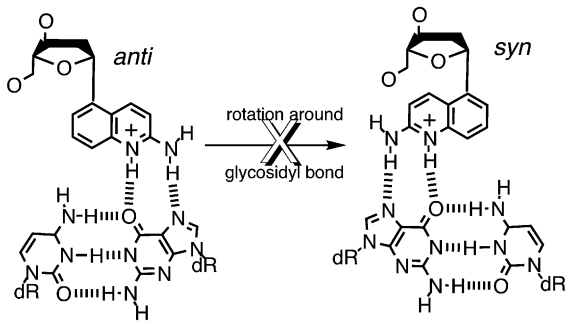

FIGURE 3: Potential rotation of antiCG (anti) into pseudo antiGC (syn).

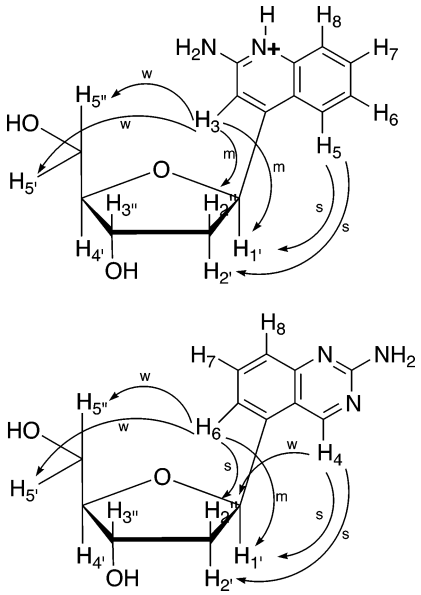

FIGURE 4: NMR NOESY analysis of antiGC (top) and antiTA (bottom) TRIPsides: s (strong); m (medium); and w (weak) NOE.

and the sugar H-1′ and H-2′ protons, and a medium NOE to H2″ (Figure 4). In addition, there is a strong interaction between the aromatic H-6 proton and the H-2″ proton, a medium interaction with H-1′, and weak interactions with the H-5′ and -5″ protons. For the antiGC TRIPside, the strong NOE interactions are between aromatic ring proton H-5 and H-1′ and H-2′. Moderate NOE signals are seen between aromatic proton H-3 and H-2″ and H-1′, and weaker interactions with H-5′ and H-5″. Overall, both molecules, as predicted, appear to preferentially populate an *anti*-like conformation (*16*).

Characterization of Triplexes. OL's 1−10 (Figure 5) were prepared using a combination of antiTA, antiGC, and natural nucleobase phosphoramidite derivatives following standard solid-phase methods. OL-1 has a duplex region with two interruptions in the purine Hoogsteen H-bonding information so triplex formation requires two major groove crossovers. The potential triplex structures of all the oligomers used in this study are shown in Figure 6. OL-2, -3, and -4 are similar to OL-1, except OL-2 and OL-4 each have one mismatch, and OL-3 has two mismatches between the TFO segment and the duplex. OL-5 has a single crossover between the purine containing strands, while OL-6, similar to OL-1, has two crossovers. Triplex formation was assayed by measuring the changes in absorbance at three different wavelengths as a function of temperature in 10 mM sodium phosphate buffer

OL-1: 5'-[antiGC]$_3$-[antiTA]-[antiGC]$_2$-C_5-G_2-T-G_3-C_5-C_3-A-C_2

OL-2: 5'-[antiGC]$_3$-[antiTA]-[antiGC]$_2$-C_5-G_2-T-C-G_2-C_5-C_2-G-A-C_2

OL-3: 5'-[antiGC]$_3$-[antiTA]-[antiGC]$_2$-C_5-G-C-T-C-G_2-C_5-C_2-G-A-G-C

OL-4: 5'-[antiGC]$_3$-[antiTA]-[antiGC]$_2$-C_5-G-C-A-C-G_2-C_5-C_2-G-T-G-C

OL-5: 5'-[antiGC]$_3$-[antiTA]$_3$-C_5-T_3-G_3-C_5-C_3-A_3

OL-6: 5'-[antiTA]$_2$-[antiGC]-[antiTA]$_3$-C_5-T_3-G-T_2-C_5-A_2-C-A_3

OL-7: 5'-G_2-T-G_3-C_5-C_3-A-C_2

OL-8: 5'-C_2-G_2-T-G_3-C_5-C_3-A-C_2

OL-9: 5'-C_5-G_2-T-G_3-C_5-C_3-A-C_2

OL-10: 5'-[antiTA]$_6$-C_5-T_6-C_5-A_6

FIGURE 5: Sequences of oligomers.

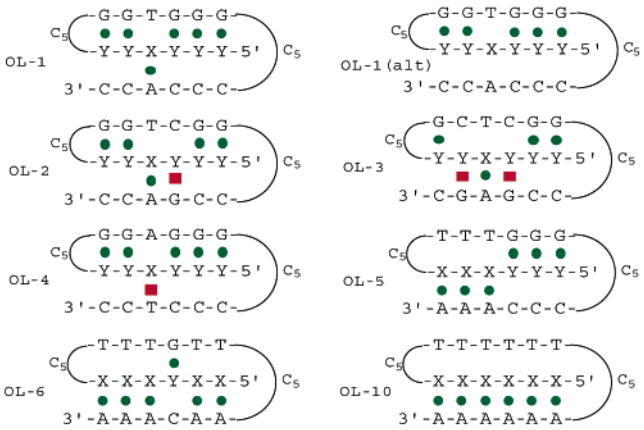

FIGURE 6: Potential triplex structures of OL's 1−6 and 10: Y = antiGC and X = antiTA; Hoogsteen H-bond (circles); Hoogsteen-duplex mismatch (squares).

(pH 7.0) containing 50 mM NaCl. The antiTA and antiGC heterocycles have λ_{max} near 350 and 330 nm, respectively. Therefore, the unstacking of the antiTA and antiGC TRIPsides from a triplex structure can be detected by observing an increase in the absorbance at 350 or 330 nm with increasing temperature. AntiTA and antiGC also fluoresce when excited at their visible absorption band. The changes in the fluorescence intensity of the oligomers at low (0 °C) and high (88 °C) temperature is also diagnostic of structure since the stacking of the antiGC and antiTA C-glycosides in a triplex will cause a significant increase in the fluorescence intensity (*16*).

The results of the UV−vis melts for OL's 1−4 are shown in Figure 7, and the T_M's calculated by first derivative and curve shape (*19*) analyses are presented in Table 1. At pH 7.0, the most stable structure is OL-1 that has a T_M above 60 °C based on the melting curves at 260, 330, and 350 nm (Table 1). The hyperchromicities at the three wavelengths is 16, 11, and 9%, respectively. *The clear and consistent transitions at all the wavelengths is evidence that OL-1 forms a stable triplex at a mixed purine/pyrimidine sequence, and that it unfolds in a single cooperative process*. Moreover, the stability of the triplex is highly dependent on sequence. A single antiGC−C:G mismatch between the TFO segment and the duplex (OL-2) results in a decrease in cooperativity

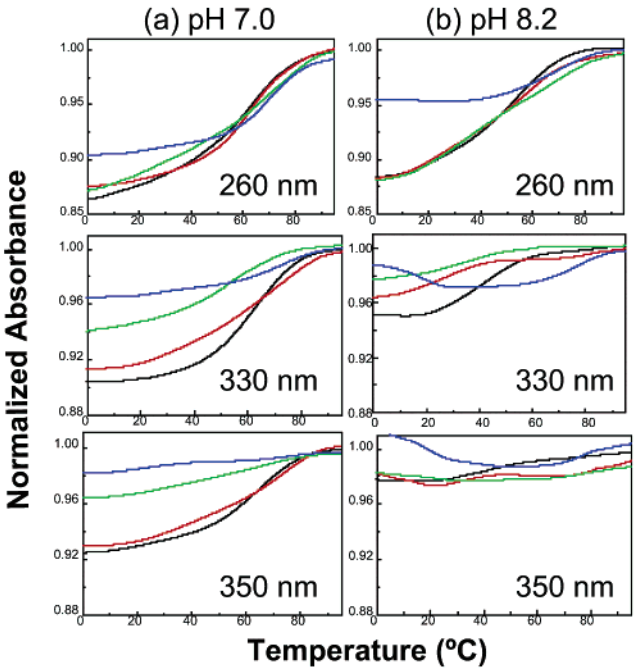

FIGURE 7: UV−vis melting studies and pH dependency of OL's 1−4 at 3−6 μM strand concentration in 10 mM sodium phosphate buffer containing 50 mM NaCl (*x*-axis, temperature; *y*-axis, absorbance): OL-1 (black), OL-2 (red), OL-3 (blue), and OL-4 (green) (see Figure 6 for sequences) at pH 7.0 (a) and 8.2 (b) at 260, 330, and 350 nm.

Table 1: T_M of Oligomers Based on Electronic Spectra[a]

		λ (nm)		
OL	pH	260	330	350
OL-1	7.0	63.7	62.8	63.1
	8.2	55.2	43.2	43.4
OL-2	7.0	62.7	55.6	58.7
	8.2	21.3	27.8	n.d.[b]
OL-3	7.0	70.2	n.d.	n.d.
	8.2	68.9	n.d.	n.d.
OL-4	7.0	70.3	52.1	n.d.
	8.2	64.3	32.4	n.d.
OL-5	7.0	44.6	45.0	44.9
	8.2	40.1	20.6	n.d.
OL-6	7.0	35.6	34.7	34.3
	8.2	30.2	21.1	20.5
OL-10[c]	7.0	26.3		24.7

[a] Values (±1 °C) based on first derivative and shape analysis (ref 8) of melting curves (Figures 8 and 9): 10 mM NaH_2PO_4 buffer (pH 7.0) containing 50 mM NaCl. [b] n.d. = not detected. [c] Data from ref 19.

and a reduction in the T_M from 63 to 57 °C at 330 nm (Table 1). The hyperchromicity is 11 and 8% at 330 and 350 nm, respectively. In this case, there appears to be a decoupling of the triplex to duplex and duplex to random coil transitions. The presence of two mismatches between the Watson−Crick duplex and antiGC in the TFO (OL-3) results in a significant decrease in the T_M, and loss of melting cooperativity and hyperchromicity (<4%) based on the spectra at 330 and 350 nm (Figure 7).

OL-4 was prepared to obtain evidence that the TFO segment in OL-1 simultaneously binds to purines in both complementary strands of the duplex target. OL-4 contains a single T:A to A:T transversion relative to OL-1. If the TFO segment is not binding to the T:A base pair, and only associated with the G:C pairs, there should be little if any

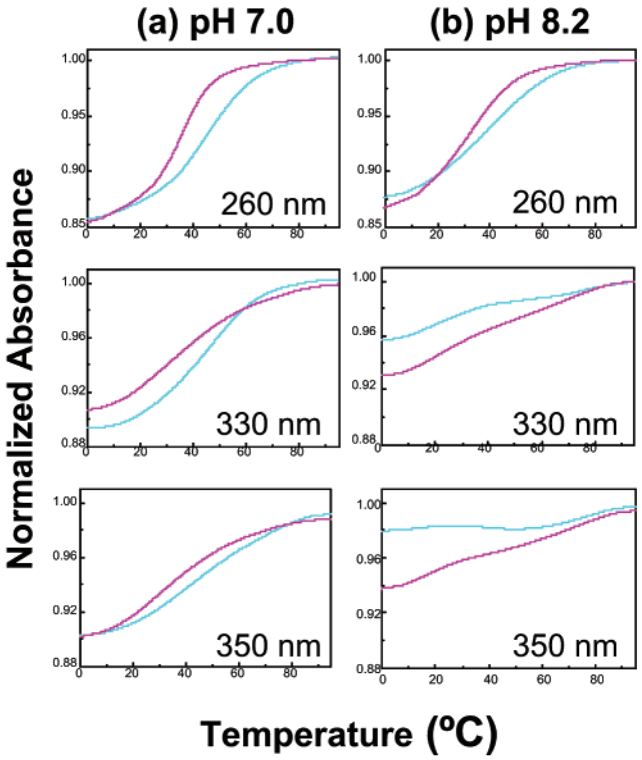

FIGURE 8: Thermal melting studies of OL-5 (blue) and OL-6 (magenta) in 10 mM sodium phosphate buffer (a) pH 7.0 and (b) pH 8.2 containing 50 mM NaCl at 260, 330, and 350 nm.

difference between the melting curves of OL-1 and OL-4. The experiment at pH 7.0 shows that this mismatch highly destabilizes the triplex: the T_M drops to approximately 52 °C at 330 nm (ΔT_M = 10.7 °C), the cooperativity is diminished, and the hyperchromicity is reduced to 6 and 4% at 330 and 350 nm, respectively (Figure 7).

OL-5, which has a single crossover, also forms a stable triplex at pH 7.0 with a T_M of 45 °C (Figure 8). In this case, the hyperchromicity is 18% at 260 nm, and 12 and 11% at 330 and 350 nm, respectively. A triplex is also seen with OL-6 that has two crossovers: T_M near 34 °C with 18% hyperchromicity at 260 nm and 10% at 330 and 11% at 350 nm (Figure 8). Despite the differences in the T_M's, all the oligomers that do not have a mismatch unfold from a triplex directly to a random coil. In contrast, the introduction of mismatches between the duplex and TFO uncouples the two transitions since the T_M's at the different wavelengths are not the same (Table 1).

Differential Scanning Calorimetry Studies. The DSC melting curves for OL-1 and the duplex control sequences are presented in Figure 9 with the calculated thermodynamic profiles shown in Table 2. The controls for OL-1 include a perfect hairpin (OL-7), one with a 5′-C_2 tail (OL-8) and one with a 5′-C_5 tail (OL-9). The T_M for OL-1 as measured by DSC shows a single transition and is within experimental error of the value derived from the UV−vis melt. The symmetry of the DSC curve also confirms the intramolecular nature of the folded OL-1 triplex (*19*). Significantly, the ΔH_{cal} for OL-1, which forms a triplex based on the electronic spectrum, is 88 kcal mol^{-1} or roughly twice the value measured for the three hairpin control duplexes (OL's 7−9).

pK_a Studies. The pK_a of antiGC was determined by measuring the change in its UV spectrum as a function of

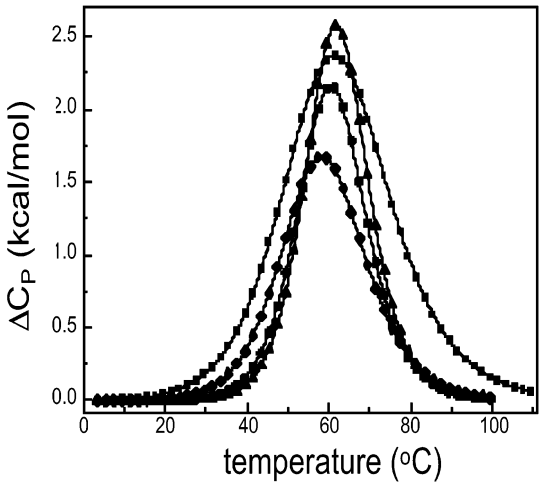

FIGURE 9: Differential scanning calorimetry profiles for the unfolding of OL's 1 and 7−9 in 10 mM sodium phosphate buffer (pH 7.0) containing 50 mM NaCl: OL-1 (squares); OL-7 (circles); OL-8 (triangles); and OL-9 (diamonds).

Table 2: Thermodynamic Profiles for the Helix−Coil Transition of OL's 1 and 7−9[a]

OL	T_M	ΔH_{cal}	$\Delta G°_{cal}$ (293 °K)	$T\Delta S_{cal}$
OL-1	62.0	88.0	11.0	77.0
OL-7	60.8	48.0	5.9	42.1
OL-8	62.0	52.7	6.6	46.1
OL-9	58.8	45.8	5.4	40.4

[a] All values obtained in 10 mM sodium phosphate buffer (pH 7.0) containing 50 mM NaCl. Experimental errors are indicated in parentheses as follows: T_M (±0.5 °C); ΔH_{cal} (±3%), $T\Delta S$ (±3%) and $\Delta G°_{293}$ (±5%). OL's 7−9 below dashed line are control duplexes.

pH (data not shown) with a calculated pK_a of 7.2, which is close to the value of 7.3 reported for 2-aminoquinoline (*20*). Therefore, at pH 7.0 a significant fraction of antiGC should be protonated, which will allow two H-bonds to be made between the TFO and the duplex. Accordingly, raising the pH above the pK_a will decrease the fraction of antiGC that is protonated, which should destabilize the triple-stranded complex. The T_M of OL-1 determined at both 330 and 350 nm drops from 63 °C at pH 7.0 to 43 °C at pH 8.2 (ΔT_M of 20 °C) (Table 1, Figure 7). The T_M at 260 nm is 55.2 °C, so at pH 8.2 there is resolution between the triplex-to-duplex and duplex-to-random-coil transitions. A small decrease in hyperchromicity at 260 nm is observed, but there is a dramatic drop by more than 50% at 330 and 350 nm. At pH 8.2, the T_M of the hairpin duplex decreases by only 3.4 °C (data not shown). The T_M for OL-2 measured at 330 nm drops by 16 °C as the pH is raised from 7.0 to 8.2. There is no discernible transition at 350 nm, and the hyperchromicity is reduced to 4%. At the higher pH, there is no evidence for triplex formation with OL-3. At pH 8.2, OL-4 has a broad transition at 330 nm with only 3% hyperchromicity. Similarly, both OL-5 and -6 at the higher pH show noncooperative melting, low hyperchromicity (<3%), and decoupling of the transitions from triplex-to-duplex and duplex-to-random-coil. A pH versus T_M profile for OL-1 and OL-6 is shown in Figure 10. Decreasing the pH below 7.0 causes a small increase in triplex stability. Clearly, the deprotonation of the antiGC residue has a major destabilizing effect on triplex formation because of the forfeiture of one Hoogsteen H-bond and/or the loss of cationic charge.

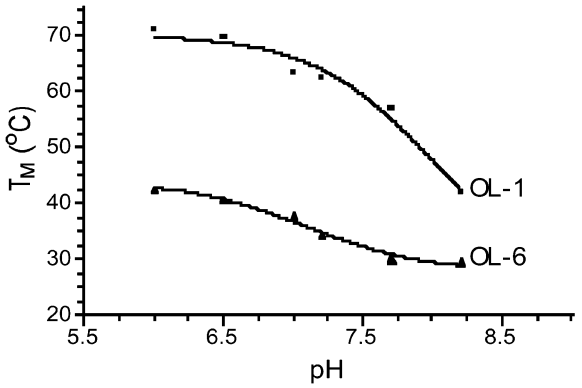

FIGURE 10: Relationship between pH and triplex stability for OL-1 and OL-6.

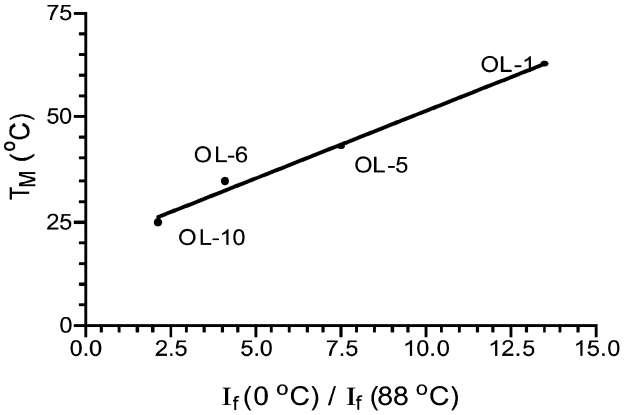

FIGURE 11: Ratio of fluorescence intensities (I_f) of intramolecular triplexes at 0 °C and 88 °C versus T_M.

Fluorescence Studies. The fluorescence of the quinazoline and quinoline heterocycles is another useful probe of their environment since there is a difference in the collisional quenching rate when the TRIPsides are exposed to solvent versus when they are part of a stable stacked structure (*16*, *21*, *22*). The fluorescence spectra at high (88 °C) and low (0 °C) temperature for the different oligomers were obtained. The ratio of the fluorescence emission λ_{max} near 430 nm (with 330 nm excitation) at the two temperatures for the perfect triplexes (OL-1, -5, -6, and -10) was plotted versus the T_M at pH 7.0 (Figure 11). OL's 2−4 were not included in the analysis because the T_M's for triplex to duplex and duplex to random coil are not coupled as is the case for the other perfect triplexes. The result of this plot is a linear response that has a correlation coefficient (r^2) of 0.99.

DISCUSSION

Conformational Analysis of antiTA and antiGC TRIPsides. Modeling of the TRIPsides bound to mixed DNA sequences suggested that the movement of the TFO backbone would be minimal while maintaining the predicted Hoogsteen base pairing needed for sequence specific recognition (*16*). The Hoogsteen base pairing scheme shown in Figure 1 requires that the TRIPside heterocycles each adopt *anti*-conformations with respect to the C-glycosidic bond (χ). If this is not the case, antiGC by rotation to the *syn*-isomer could bind to both a G:C and C:G base pair as shown in Figure 3. The same is true for antiTA binding to T:A and A:T. ^{1}H NMR NOE studies on the antiTA and antiGC TRIPsides show that they indeed have a strong preference for the predicted *anti*-conformation at physiological conditions.

Triplex Formation at Non-Homopurine Sequences. The melting results show that the triplexes without any mismatches between the duplex and TFO unfold directly to random coil, i.e., two-state transition. A two-state transition is generally observed with intramolecular triplexes for reasons previously discussed (*23*), in contrast to the three-state transition model for intermolecular triplexes. The electronic and fluorescence spectroscopy data presented for the three matched intramolecular triplexes (OL-1, OL-5, and OL-6) confirm that as many as two crossovers in the space of six base pairs does not present a barrier to the formation of stable triplex structures. The DSC results show that $\Delta\Delta G°$ (at 293 °K) for OL-1 relative to duplex controls OL's 7−9 is more than 5 kcal mol^{-1}, and the major component is the ΔH term indicating the role of TRIPside stacking in the triplex.

Most importantly, evidence is provided showing that the TFO segment concurrently reads purine information on both Watson−Crick strands. There is approximately a 10 °C decrease in the T_M at 330 nm due to the T:A to A:T transversion in the duplex target of OL-4. The nature of the base pairing scheme, i.e., A:T versus T:A, at the site where antiTA is predicted to bind would have had little effect on stability if the TFO "skipped" this position and only read the G's on one strand of the major groove (Figure 6, OL-1-alt) rather than being simultaneously Hoogsteen paired to all the purines in the duplex (Figure 6, OL-1). The introduction of an antiGC mismatch with a C:G base pair (OL-2) results in an even larger decrease in the T_M, and in fact destabilizes the triplex to the point that there is a stepwise unfolding of the triplex and duplex structures. Together, the melting experiments show that stable triplex formation with the TRIPsides involves, and in fact requires, that the TFO be sequence specifically paired with purines on both strands of the Watson−Crick duplex.

To put the UV−vis melting data into perspective, the natural triplex formed from 5′-TCTCTCT-C_5-TCTCTCT-C_5-AGAGAGA has a T_M of 37.3 °C at pH 7.0 in 16 mM NaCl (*23*). This natural triplex, which recognizes a homopurine sequence, has seven bases and three *staggered* cationic residues. OL-5, which recognizes a mixed purine/pyrimidine sequence and forms a six base pair triplex with three *consecutive* cationic residues, has a T_M of 46 °C at pH 7.0 in 50 mM NaCl. Therefore, at physiological pH, TFO's with antiGC and antiTA TRIPsides form triplexes at mixed purine/pyrimidine sequences that are at least as stable as their natural TFO counterparts at homopurine runs.

Effect of Cationic antiGC TRIPsides on Triplex Stability. Similar to the effect of protonated cytosines (at pH ≤ 6.0) in TFO sequences, the inclusion of cationic antiGC residues also has a dramatic stabilizing effect on the triplexes. For example, the introduction of one antiGC TRIPside in OL-10 to create OL-6 results in a 10 °C increase in the T_M and a significant increase in cooperativity (*16*). The T_M of the intramolecular natural triplex, i.e., 5′-TCTCTCT-C_5-TCTCTCT-C_5-AGAGAGA, at pH 6.2 in 10 mM sodium cacodylate buffer containing 16 mM NaCl is 52.6 °C (*23*). This compares to a T_M of 23.2 °C at pH 7.0 in the same buffer system for 5′-T_7−C_5−T_7−C_5−A_7. The ΔT_M of 29.4 °C represents three protonated C residues (10 °C increase

per C residue). The $\Delta\Delta G°$ between the two triplexes is 13.3 kcal mol^{-1} (4.4 kcal mol^{-1} per C$^+$-G:C triplet) (*23*). It should be noted that the thermodynamic comparison of the triplex stabilities cannot be simply correlated to the number of protonated cytosines since the triplet stacking arrangements in the two oligomers are very different because of the dissimilar sequences. In other studies, the formation of a C$^+$-G:C triplet has a $\Delta G°$ of −3.0 kcal, a value similar to that for the formation of a G:C base pair (*24*). Depending on the flanking triplets, the C$^+$-G:C triplet is thermodynamically favored 3−4-fold over a T-A:T triplet (*24*). At neutral pH, the presence of successive cytosine residues in pyrimidine-based TFO's can actually diminish the extent of stabilization relative to TFO's with isolated cytosines due to less efficient protonation and the low pK_a of cytosine (*25*, *26*). However, at acidic pH, where the cytosines are all protonated, little, if any, destabilization is observed indicating that adjacent charges do not intrinsically affect triplex formation (*25*).

We have observed a significant destabilization of triplex formation by raising the solution pH to 8.2 as this effect is analogous to that described above for C's at pH 7.0. Lowering the pH has a much more modest stabilizing effect, and this is also understandable since the pK_a of free antiGC is 7.2. Analysis of the plots in Figure 10 show transitions at pH 7.2, indicating that the pK_a of antiGC is similar in an oligomer and monomer.

Sequence Specificity. In addition to stability, the question of sequence specificity is critical for the evolution of TFO's designed to bind to unique genomic sequences. The introduction of mismatches between the antiTA and antiGC based TFO's and duplex regions has the requisite destabilizing effect. For example, a single antiGC-C:G mismatch causes OL-2 to melt more than 7 °C lower than the perfect matched OL-1. An antiTA-A:T mismatch (OL-4) decreases stability by approximately 10 °C, which is a value similar to what we previously observed for the same type of mismatch in OL-10 (*16*). In addition, a loss of cooperativity and hyperchromicity is associated with the presence of mismatches. Similar changes in T_M have been reported for mismatches involving natural bases in an intramolecular pyrimidine motif (*27*, *28*). Since the thermodynamic penalty for mismatches with the TRIPsides is at least as large as with natural triplexes, these molecules will bind with high stringency to their Watson−Crick target. The destabilization caused by transversional mismatches is also strong evidence that the TRIPsides are in the anti-conformation in TFO's.

Relationship Between Intramolecular Triplex Structure and Monophasic Transitions. The perfect triplexes involving the TRIPsides all melt with monophasic transitions at pH 7.0 based on the similar T_M values calculated at 260, 330, and 350 nm. A similar phenomenon is observed with natural intramolecular triplexes (*23*, *24*). However, this is not the case in the mismatched oligomers, where the T_M's calculated at 260 nm versus 330 and 350 nm differ. The decoupling of the triplex-to-duplex and duplex-to-random-coil transitions is also observed in the studies performed at the higher pH of 8.2. Under these conditions, the reduced protonation of the TRIPsides yields a reduction in Hoogsteen H-bonding and a decrease in the favorable enthalpy contribution associated with TFO stacking interactions. This is compensated by an increase in the unfolding entropy contributions associated with both increased conformational flexibility of the TFO segment and the putative release of protons and cations. Furthermore, the entropy gain in the unfolding of the third strand of intramolecular triplexes is lower than that of intermolecular triplexes because this strand is already restricted in the former. The overall melting behavior, mono- versus biphasic, depends on the $\Delta H-\Delta S$ compensative relationship: the stacking interactions (enthalpy) of the TFO are released only if the entropy gain is greater (*23*). Deprotonation of antiGC at higher pH or the introduction of TFO-duplex mismatches increases the enthalpy loss and/or increases the entropy gain, and affords biphasic melting curves due to specific destabilization of the binding of the TFO. It is reassuring to observe similar thermodynamic behavior between triplexes formed from natural bases and TRIPsides.

In conclusion, UV−vis, fluorescence, and DSC evidence are presented to show that the antiTA and antiGC TRIPsides can form stable and sequence-specific intramolecular triplexes at nonhomopurine sequences. While only two of the four TRIPsides were used in this study, the ability to target any duplex DNA sequence seems achievable. Studies are underway to incorporate the remaining two TRIPsides (antiAT and antiCG) into TFO's to complete the four monomer based double-stranded DNA recognition scheme.

ACKNOWLEDGMENT

We thank Dr. Paul Keifer of the UNMC Eppley Cancer Center NMR Shared Resource for help with the NMR studies, and Greg Kubik of the UNMC Eppley Cancer Center Molecular Biology Shared Resource for the synthesis of the oligomers.

REFERENCES

1. Arnott, S., and Bond, P. J. (1973) *Nat. New Biol. 244*, 99−101.
2. Rajagopal, P., and Feigon, J. (1989) *Nature 339*, 637−640.
3. de los Santos, C., Rosen, M., and Patel, D. (1989) *Biochemistry 28*, 7282−7289.
4. Umemoto, K., Sarma, M. H., Gupta, G., Luo, J., and Sarma, R. H. (1990) *J. Am. Chem. Soc. 112*, 4539−4545.
5. Sklenár, L., and Feigon, J. (1990) *Nature 345*, 836−838.
6. Tarköy, M., Phipps, A. K., Schultze, P., and Feigon, J. (1998) *Biochemistry 37*, 5810−5819.
7. Felsenfeld, G., Davies, D. R., and Rich, A. (1957) *J. Am. Chem. Soc. 79*, 2023−2024.
8. Morgan, A. R., and Wells, R. D. (1968) *J. Mol. Biol. 37*, 63−80.
9. Lee, J. S., Johnson, D. A., and Morgan, A. R. (1979) *Nucleic Acids Res. 6*, 3073−3091.
10. Moser, H. E., and Dervan, P. B. (1987) *Science 238*, 645−650.
11. Broitman, S. L., Im, D. D., and Fresco, J. Y. (1987) *Proc. Natl. Acad. Sci. U.S.A. 84*, 5120−5124.
12. Cooney, M., Czernuszewicz, G., Postel, E. H., Flint, S. J., and Hogan, M. E. (1988) *Science 241*, 456−459.
13. Kohwi, Y., and Kohwi-Shigematsu, T. (1988) *Proc. Natl. Acad. Sci. U.S.A. 85*, 3781−3785.
14. Beal, P. A., and Dervan, P. B. (1991) *Science 251*, 1360−1363.
15. The C-glycosides shown in Figure 1 are referred to as TRIPsides for the 2′-deoxyribose-substituted compounds. All other standard nucleotide nomenclature is maintained.
16. Li, J.-S., Fan, Y.-H., Zhang, Y., Marky, L. A., and Gold, B. (2003) *J. Am. Chem. Soc. 125*, 2084−2093.
17. Hardman, R., and Partridge, M. W. (1954) *J. Chem. Soc. 1954*, 3878−3884.
18. Farr, R. N., and Davies, G. D., Jr. (1990) *Carbohydr. Chem. 9*, 653−660.
19. Marky, L. A., and Breslauer, K. J. (1987) *Biopolymers 26*, 1601−1620.
20. Perrin, D. D. *Dissociation Constants of Organic Bases in Aqueous Solution*, Butterworth Press, London, 1965.

21. Lyckell, P.-O., Gräslund, A., Claesens, F., McLaughlin, L. W., Larsson, U., and Rigler, R. (1987) *Nucleic Acids Res. 15*, 9011−9025.
22. Wu, P., Nordlund, T. M., Gildea, B., and McLaughlin, L. W. (1990) *Biochemistry 29*, 6508−6514.
23. Soto, A. M., Loo, J., and Marky, L. A. (2002) *J. Am. Chem. Soc. 124*, 14355−14363.
24. Roberts, R. W., and Crothers, D. M. (1996) *Proc. Natl. Acad. Sci. U.S.A. 93*, 4320−4325.
25. Leitner, D., Schroder, W., and Weisz, K. (2000) *Biochemistry 39*, 5886−5892.
26. Sugimoto, N., Wu, P., Hara, H., and Kawamoto, Y. (2001) *Biochemistry 40*, 9396−9405.
27. Roberts, R. W., and Crothers, D. M. (1991) *Proc. Natl. Acad. Sci. U.S.A. 88*, 9373−9401.
28. Soto, A. M., and Marky, L. A. (2002) *Biochemistry 41*, 12475−12482.

BI035648D